Journal of Sound and Vibration 333 (2014) 4073–4083

Contents lists available at ScienceDirect

Journal of Sound and Vibration

journal homepage: www.elsevier.com/locate/jsvi

$\mathcal{H}_2$ optimal vibration control using inertial actuators and a comparison with tuned mass dampers

N. Alujević [a], G. Zhao [a,*], B. Depraetere [b], P. Sas [a], B. Pluymers [a], W. Desmet [a]

[a] KU Leuven, Production Engineering, Machine Design and Automation (PMA) Section, Celestijnenlaan 300b – Box 2420, 3001 Heverlee, Belgium

[b] FMTC, Flanders' Mechatronics Technology Centre, Celestijnenlaan 300d – Box 4027, 3001 Heverlee, Belgium

ARTICLE INFO

Article history:
Received 28 August 2013
Received in revised form
19 February 2014
Accepted 18 April 2014
Handling Editor: J. Lam
Available online 14 May 2014

ABSTRACT

The optimum resonance frequency and the damping coefficient for passive Tuned Mass Dampers (TMD) have been determined using various optimality criteria in the past. In this study an active damping method using Inertial Actuators (IAs) is considered. Closed form expressions for the $\mathcal{H}_2$ optimal control parameters that minimise the kinetic energy of the primary structure are derived. It is shown that the resonance frequency of the IA should be as low as practically possible. However, for a given resonance frequency, an optimal pair exists of the passive damping coefficient of the IA and the feedback gain. Closed form expressions for these are provided in the paper. It is noted that the amount by which the described active approach outperforms an optimally tuned TMD having the same mass depends on the squared ratio of resonance frequencies of the IA and the primary structure.

1. Introduction

Vibration control using absorbers is an interesting option for reducing vibrations of various types of mechanical structures. The attractiveness of the method is that a relatively small extra mass carefully suspended in the primary structure can lead to significantly reduced responsiveness of the primary structure to forcing [1–4]. The mass is added to the primary structure via a coupling that can often be approximately represented through a spring–dashpot pair.

Depending on whether the excitation of the primary structure is at a single frequency or comes in a broad range of frequencies, the coupling is designed using different principles. For example, in the case of simple harmonic excitations at a single frequency, the stiffness of the absorber coupling can be set such that the resonance frequency of the suspended mass–spring system equals the excitation frequency. If the absorber damping can be set very low, then its addition to the primary structure generates virtually a zero in the primary structure input receptance at the excitation frequency. Thus the primary structure becomes unresponsive to harmonic forces acting at the absorber mass–spring resonance frequency. This type of absorber is often referred to as a vibration neutraliser. A lot of research work has been carried out on how to tune the resonance frequency of vibration neutralisers to varying excitation frequencies [5–21], and some work has also been done on how to achieve a very low damping in the neutraliser, see for example [22].

On the other hand, if the primary disturbance covers a broad frequency range, for example in cases of aerodynamic loading, vehicle road excitations, earthquakes, or impacts, then adding a zero at a single frequency is not necessarily useful.

* Corresponding author.
E-mail address: nudt.guoying@gmail.com (G. Zhao).

http://dx.doi.org/10.1016/j.jsv.2014.04.038
0022-460X/

This is because the driving point receptance of the coupled system taken at the primary structure presumably has also got poles where its amplitudes can be very large and thus the response of the primary structure can be large, too. In such cases the damping and the stiffness of the absorber could be tuned such that certain vibration metrics are minimised in the frequency band of interest. Devices with such tuned stiffness and damping are known as TMDs. Some of the earliest studies on how to tune the stiffness and the damping of a TMD are given in [1,4]. The metrics used were the vibration amplitudes at resonances, and accordingly the stiffness and the damping of the TMD were set to minimise the maximum response of the primary structure, that is, to minimise the response at resonances. This is in fact an $\mathcal{H}_\infty$ optimisation of the coupled system composed by the TMD and the primary structure where the optimisation parameters are the TMD stiffness and the damping coefficient [1,23].

Alternative valid metric for vibrations of the primary structure is the kinetic energy of the primary structure which is proportional to its average squared vibration velocity. In this case the optimisation can be performed as well, and it yields a different set of optimal stiffness and damping of the TMD. This is in fact an $\mathcal{H}_2$ optimisation of the coupled system composed by the TMD and the primary structure where the primary structure kinetic energy is minimised. This type of optimisation has been performed by Warburton [24]. There are also other possible optimality criteria that can be of interest and some of the relevant studies can be found in [25–29].

Considering their mechanical layout, TMDs are rather similar to IAs. However, in addition to the passive elastic and damping forces in the coupling, an active force can be generated between the inertial actuator proof mass and the primary structure. The force can be made proportional to the primary structure velocity via a fixed negative feedback gain. In this case an amount of active damping can be generated on the primary structure [30,31]. Such control is an active approach and thus the stability of the feedback loop needs to be addressed as well. In fact, for stability reasons, it is required that a certain amount of relative damping between the primary structure and the proof mass is employed in parallel to the active, absolute damping [31,32]. Furthermore, there is a maximum ratio between the active (absolute) and the passive (relative) damping which must not be exceeded in order to keep the feedback loop stable [32,33].

This study is focused on the described active damping approach where a damped IA is added to an otherwise undamped primary structure and its force generator is driven with a signal proportional to the primary structure absolute velocity. It is shown that there is an $\mathcal{H}_2$ optimal combination of the passive and the active damping which, when employed, minimises the kinetic energy of the primary structure. These passive and the active damping ratios are calculated in the closed form. It is shown that the optimal active to passive damping ratio is about two-thirds of the maximal ratio allowed by stability requirements. This means the existence of gain and phase margins. Finally, the kinetic energy of the primary structure under $\mathcal{H}_2$ optimal active control is compared to that under $\mathcal{H}_2$ optimal passive control using TMDs having the same proof mass. A comparison of the two control effects reveals that the active control can significantly outperform the passive control provided that the resonance frequency of the IA is made low. In fact, the optimally tuned IA outperforms the optimally tuned TMD having equal mass by an extent which increases with the reduction of squared resonance frequency of the IA.

The paper is structured into 6 sections. In Section 2 the model problem studied and the mathematical formulation are given, and in Section 3 the $\mathcal{H}_2$ optimal active control parameters using IAs are derived. A discussion of relative stability is presented in Section 4. Finally, Section 5, which gives the comparison of the passive and active control effects, is followed by the conclusions.

2. Model problem and mathematical formulation

The inertial actuator is used to implement a velocity feedback loop which comprises a velocity sensor mounted onto the primary structure and a force actuator parallel to the passive mount. The output of the sensor is amplified by a negative gain and fed back to the actuator (Fig. 1).

As can be seen in Fig. 1, the primary structure is modelled as an undamped, lumped parameter one degree of freedom (dof) system, defined through the mass m_1 and the stiffness k_1. It is excited by the primary excitation force f_p, which is assumed to be a white noise random force with the flat spectral amplitude equal to unity.

Next, the kinetic energy of the primary structure is calculated and its dependence on the passive and active control parameters is established. A dimensionless parameter I_k is introduced to represent the kinetic energy, which is defined as the ratio of the kinetic energy of the primary system to the excitation force with a uniform power spectral density $S_f(\omega)$ [29]:

$$I_k = \frac{m_1 E[|v_1|^2]}{2S_f\omega_1/k_1}, \tag{1}$$

where $E[\,]$ denotes the expectation value, v_1 is the velocity of the primary structure, and ω_1 is the circular resonance frequency of the primary structure. The mean squared value of the velocity of the primary structure can be expressed as

$$E[|v_1|^2] = \frac{S_f\omega_1}{m_1k_1}\int_{-\infty}^{+\infty} |Y_{1,p}|^2 \mathrm{d}\Omega, \tag{2}$$

where $\Omega = \omega/\omega_1$ is the dimensionless frequency and $Y_{1,p}$ is the dimensionless driving point mobility of the primary system defined as

$$Y_{1,p}(\Omega) = \sqrt{k_1m_1}\frac{v_1}{f_p}(\mathrm{i}\Omega). \tag{3}$$

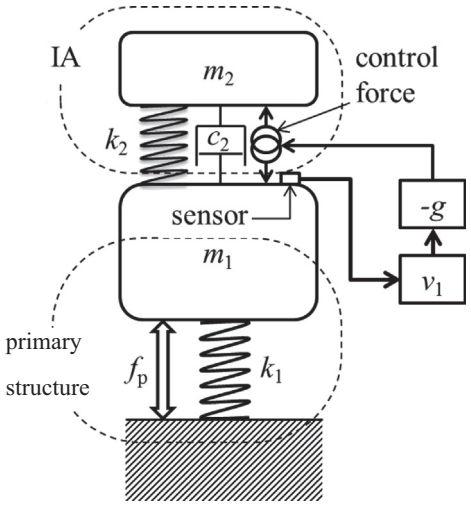

Fig. 1. The schematic of the active vibration control using an IA and a velocity feedback loop.

From Eqs. (1)–(3) the kinetic energy of the primary mass excited by a white noise spectrum of unit amplitude is given by

$$I_k = \frac{1}{2}\int_{-\infty}^{+\infty} |Y_{1,p}|^2 \mathrm{d}\Omega. \tag{4}$$

The non-dimensional driving point mobility for the active control with the IA can be expressed as

$$Y_{1,p} = \frac{-\mathrm{i}\Omega^3 - 2\eta f\Omega^2 + \mathrm{i}\Omega f^2}{\Omega^4 - 2\mathrm{i}(1+(\xi+1)\mu)f\eta\Omega^3 - (1+(\mu+1)f^2)\Omega^2 + 2\mathrm{i}\Omega\eta f + f^2}, \tag{5}$$

where $\mathrm{i}=\sqrt{-1}$, $\mu = m_2/m_1$, $f = \sqrt{k_2 m_1/k_1 m_2}$, $\eta = c_2/2\sqrt{k_2 m_2}$, $\xi = g/c_2$ and g is the feedback gain.

According to [34] the performance index I_k can be calculated as

$$I_k^{\mathrm{IA}} = \frac{\pi(1+(\mu\xi+1+\mu)f^4+(4\eta^2-\mu\xi-2)f^2)}{2\eta\mu f(\xi+1-\xi(\mu\xi+1+\mu)f^2)}. \tag{6}$$

3. $\mathcal{H}_2$ optimal active control using IAs

In this section the $\mathcal{H}_2$ optimal active control parameters are derived in the closed form. Eq. (6) gives the performance index I_k^{IA} as a function of the system parameters. Assuming that the resonance frequency f is fixed, the optimal values of η and ξ to minimise the performance index I_k^{IA} are derived by solving the following system of equations for η and ξ:

$$\frac{\delta I_k^{\mathrm{IA}}}{\delta\eta}(f,\eta,\xi) = 0, \tag{7}$$

$$\frac{\delta I_k^{\mathrm{IA}}}{\delta\xi}(f,\eta,\xi) = 0 \tag{8}$$

or

$$1+(\mu\xi+\mu+1)f^4+(-4\eta^2-2-\mu\xi)f^2 = 0, \tag{9}$$

$$[(\xi+1)\mu+1]^2 f^6 + [(-4\xi-2+8\xi\eta^2+4\eta^2)\mu-3+4\eta^2-\mu^2\xi^2]f^4 + (2\mu\xi-4\eta^2+3)f^2 - 1 = 0. \tag{10}$$

Then the optimal active and passive damping ratios can be calculated as

$$\eta_{\mathrm{opt}}^{\mathrm{IA}} = \frac{\sqrt{6[(\mu+1)f^4+(\mu-2)f^2+\sqrt{p}+1]}}{12f}, \tag{11}$$

$$\xi_{\mathrm{opt}}^{\mathrm{IA}} = \frac{\sqrt{p}-5-(5+5\mu)f^4+(10+\mu)f^2}{6\mu f^2(f^2-1)}, \tag{12}$$

where $p=1+(\mu+1)^2f^8+(14\mu^2-2\mu-4)f^6+(\mu^2-2\mu+6)f^4+(2\mu-4)f^2$ is a substitution to shorten the expressions. The performance index under optimal setting can be expressed as

$$I^{\mathrm{IA}}_{k,\mathrm{opt}}=\frac{3\pi\sqrt{6}f^2(f+1)^2(f-1)^2\sqrt{(\mu+1)f^4+(\mu-2)f^2+p+1}}{(\mu+1)^2f^8-(4+2\mu+10\mu^2)f^6+[\mu^2+(p-2)\mu+6+p]f^4+(\mu-2)(p+2)f^2+p+1}. \tag{13}$$

The optimisation has been performed without considering the frequency ratio as an optimisation parameter. However, as shown in Fig. 2, where the optimal performance index, as defined in Eq. (13), is plotted against the mass and the frequency ratio, there is no optimal frequency ratio. On the contrary, there is a frequency ratio that is to be avoided, especially for small mass ratios, where the optimal performance index increases. This frequency ratio is close to unity.

The lowest levels of the optimal performance index are in the range where the frequency ratio is below one. In this range the trend is that a decrease in the performance index comes with a decrease in the frequency ratio. The mass ratio would normally be well below unity for a lightweight IA; that is, only a small mass would be added to control vibrations of the primary structure. Thus, the lower the frequency ratio, the better the reduction in the performance index. The lower limit on the frequency ratio can be imposed by practical problems related to designing very compliant springs k_2 combined with the small size of the actuator (see for example [30]). Also, as discussed later in the paper, the phase margin of the system under active control tends to decrease as the frequency ratio is lowered.

In conclusion, the frequency ratio and the mass ratio should be below one: the mass ratio due to the lightweight design, and the frequency ratio for better performance. If they are set to be considerably smaller than one, then it is possible to approximate expressions (11)–(13) in order to obtain simpler and more easily interpretable relations. Developing expressions (11)–(13) into series with respect to the frequency ratio f and keeping only the lowest-order terms yield approximate expressions for optimal control with reasonable accuracy for a lightweight, low frequency IA:

$$(\eta^{\mathrm{IA}}_{\mathrm{opt}})_{f\ll1,\mu\ll1}\approx\frac{\sqrt{3}}{6f}, \tag{14}$$

$$(\xi^{\mathrm{IA}}_{\mathrm{opt}})_{f\ll1,\mu\ll1}\approx\frac{2}{3\mu f^2}, \tag{15}$$

$$(I^{\mathrm{IA}}_{k,\mathrm{opt}})_{f\ll1,\mu\ll1}\approx3\pi\sqrt{3}f^2. \tag{16}$$

The relative errors introduced by the approximations are below 5 percent up to the mass and frequency ratios of 20 percent.

The exact optimal control parameters as given in Eqs. (11)–(13) are shown in Fig. 3. The shapes of the three plots indicate why approximations (14)–(16) are reasonable. For example, the optimal passive damping ratio does not depend much on the mass ratio, so the simplified expression given in Eq. (14) does not include the mass radio.

Next, the effects of using the IA with velocity feedback are illustrated on an example system where both the mass ratio and the frequency ratio are set to 0.1. The passive damping ratio is set to optimality according to Eq. (11). Fig. 4(a) shows the primary structure driving point mobility plotted against frequency for six different active damping ratios: 0, 1/20 1/5, 1/2, 1, and 3/2. Fig. 4(b) shows the primary structure performance index plotted against the normalised active damping ratio $\xi/\xi^{\mathrm{IA}}_{\mathrm{opt}}$.

It can be seen in Fig. 4(a) that as the active damping ratio is increased from zero, vibrations of the primary structure are reduced at the primary structure resonance at $\Omega=1$. As the active damping is further increased, a new resonance peak occurs around $\Omega=0.1$, which is the resonance of the IA. As shown in Fig. 4(b), this causes the performance index I^{IA}_{k} to increase from its minimum value at $\xi^{\mathrm{IA}}_{\mathrm{opt}}$ towards infinity as the active damping ratio approaches 3/2. If the optimal active damping ratio is implemented, then the performance index is minimised as can be seen in Fig. 4(b).

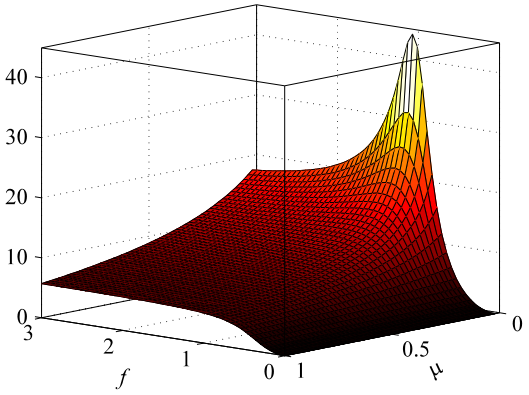

Fig. 2. The optimal performance index $I^{\mathrm{IA}}_{k,\mathrm{opt}}$ plotted against the mass ratio and the frequency ratio.

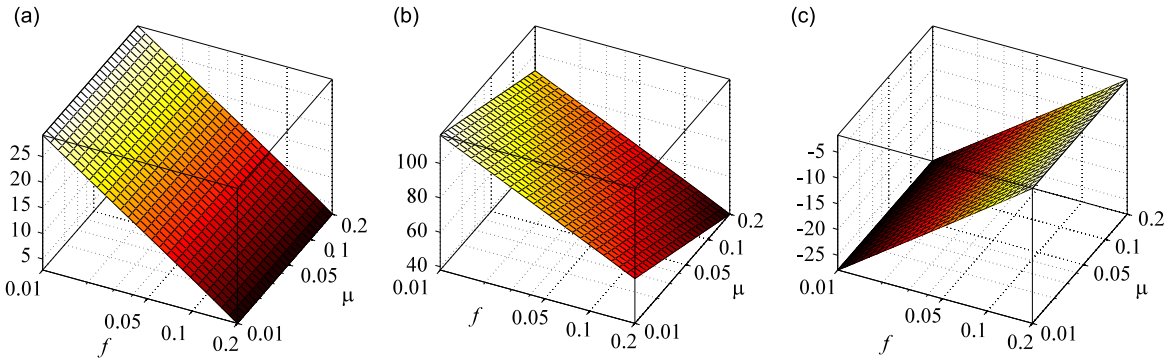

Fig. 3. The exact $\mathcal{H}_2$ optimal parameters: (a) is the optimal passive damping ratio (dB), (b) is the optimal active damping ratio (dB), and (c) is for the performance index $I^{IA}_{k,opt}$ under the optimal setting (dB).

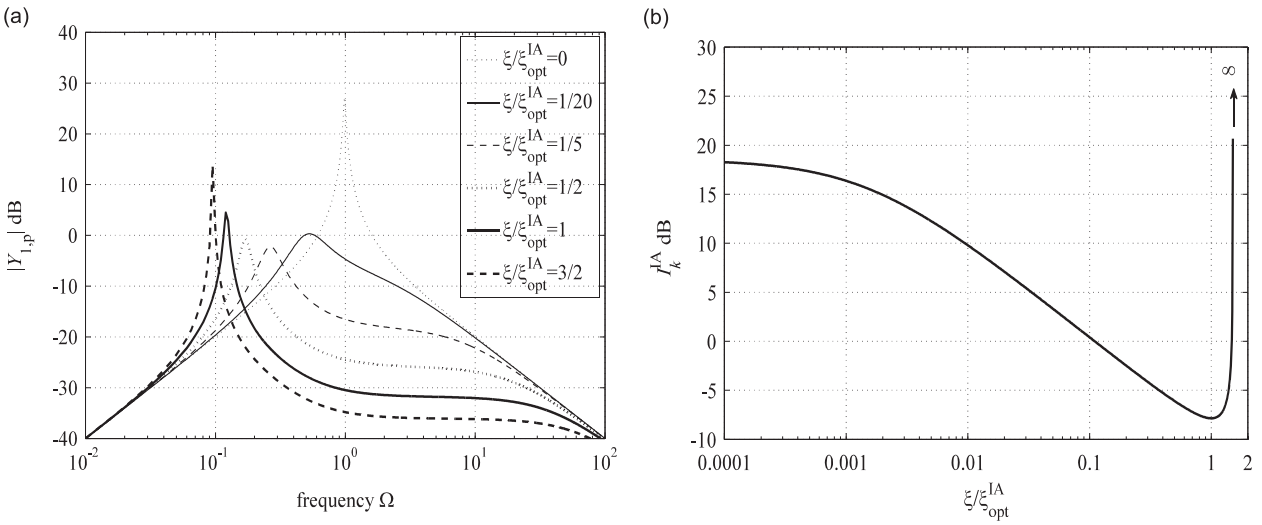

Fig. 4. (a) The driving point mobility of the primary structure under different active damping ratios and (b) the performance index plotted against the normalised active damping ratio. The passive damping ratio is kept constant and set to the optimal value.

The same example system is used next to illustrate the evolution of the performance index I^{IA}_k against the passive and the active control parameters. Fig. 5 shows the performance index I^{IA}_k plotted against the normalised passive damping ratio η and the active to passive ratio ξ. An abrupt increase in the performance index I^{IA}_k can be seen as the normalised active damping ratio approaches 1.5, suggesting that the system may be touching on the verge of a stability limit. Also, in Fig. 4(a) the increased primary structure response around the IA resonance indicates control spillover, an effect that usually precedes the breach of the stability limit.

For these reasons the stability of the active system needs to be addressed as well. Although it is guaranteed if the optimal active damping ratio is used, it is not clear what the gain and the phase margins are in such a case. In the forthcoming part of the study it is shown that relative active to passive damping ratios exist that define the bordering line between stable and unstable systems. In particular, it is shown that the $\mathcal{H}_2$ optimal systems are at a distance from this line.

4. Relative stability of the $\mathcal{H}_2$ optimal active control using IAs

The stability of an active system can be studied by applying the Routh–Hurwitz criterion to its closed loop characteristic equation [35]. This yields a system of four inequalities arising from the requirement that the four principal diagonal minors of the Routh–Hurwitz array are positive:

$$\xi > -1-\frac{1}{\mu}, \tag{17}$$

$$\xi > -1-\frac{1}{\mu}+\frac{1}{\mu(\mu f^2+f^2+1)}, \tag{18}$$

$$\xi > \frac{1-\mu f^2-f^2-\sqrt{(1-\mu f^2-f^2)^2+4\mu f^2}}{2\mu f^2}, \tag{19}$$

$$\xi < \frac{1-\mu f^2-f^2+\sqrt{(1-\mu f^2-f^2)^2+4\mu f^2}}{2\mu f^2}. \tag{20}$$

Taking into account the fact that the mass ratio μ, the frequency ratio f, and, in principle, the active damping ratio ξ are positive real numbers, it is possible to see that any positive real ξ satisfying inequality (18) automatically satisfies inequality (17). Also the condition in inequality (19) is stricter than the condition in inequality (18). The proof is given in Appendix A of this paper. Furthermore, Eq. (20) gives the maximum negative active damping stability limit if the feedback loop applying positive velocity feedback is used (a sort of active "undamping").

In conclusion, the range of ξ where the stability requirements are satisfied is given by inequalities (19) and (20):

$$\frac{-\mu f^2-f^2+1-\sqrt{(-\mu f^2-f^2+1)^2+4\mu f^2}}{2\mu f^2} < \xi < \frac{-\mu f^2-f^2+1+\sqrt{(-\mu f^2-f^2+1)^2+4\mu f^2}}{2\mu f^2}. \tag{21}$$

In order to simplify the expressions given in Eq. (21), the boundaries for the maximal/minimal active damping ratio can be developed into Taylor series with respect to the frequency ratio f such that the expressions in (21) are approximated using the lowest-order terms of the expansion. Consequently they shorten to

$$-1 < \xi < \frac{1}{\mu f^2}, \tag{22}$$

where the maximum positive active to passive damping ratio is defined as the critical active to passive damping ratio $\xi^{\mathrm{IA}}_{\mathrm{crit}} = 1/\mu f^2$. The critical active to passive damping ratio $\xi^{\mathrm{IA}}_{\mathrm{crit}}$ calculated here is identical to that given in [32].

On the other hand, the maximum negative active to passive damping ratio (the minimum) is around -1, as shown by Eq. (22); that is, the system will go unstable if the negative active damping cancels the passive damping generated by dashpot c_2.

The approximated optimal active to passive damping ratio is about 2/3ds of the approximated critical one. This is an equivalent of a 3.5 dB gain margin which is independent of the parameters of the primary structure and the absorber as long as the resonance frequency of the absorber is significantly below the resonance frequency of the primary structure. The gain margin of an active system can also be seen from the kinetic energy point of view in Fig. 4(b) and in Fig. 5, which both indicate that I_k^{IA} rapidly increases when the feedback gain approaches its critical value of 150 percent of the optimal value.

Considering now the phase margin, it can be better interpreted using the Nyquist stability criterion. The phase margin is given by

$$\mathrm{PM} = \pi + \angle\{G(\mathrm{i}\Omega_{\mathrm{gc}})H(\mathrm{i}\Omega_{\mathrm{gc}})\}, \tag{23}$$

where $G(\mathrm{i}\Omega)$ is the dimensionless sensor–actuator open loop frequency response function, $H(\mathrm{i}\Omega)$ is the dimensionless frequency response function of the feedback controller, and Ω_{gc} stands for the dimensionless gain crossover frequency. The gain crossover frequency is given by

$$|G(\mathrm{i}\Omega_{\mathrm{gc}})H(\mathrm{i}\Omega_{\mathrm{gc}})| = 1. \tag{24}$$

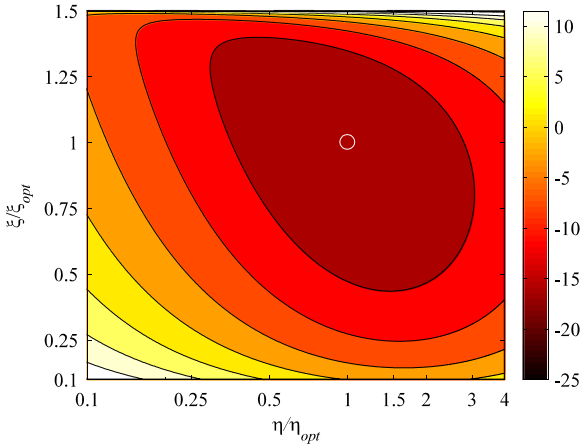

Fig. 5. The performance index I_k^{IA} (dB) plotted against the normalised passive damping ratio η/η_{opt} and the normalised active to passive damping ratio $\xi/\xi^{\mathrm{IA}}_{\mathrm{opt}}$ with $\mu = 0.1$ and $f = 0.1$.

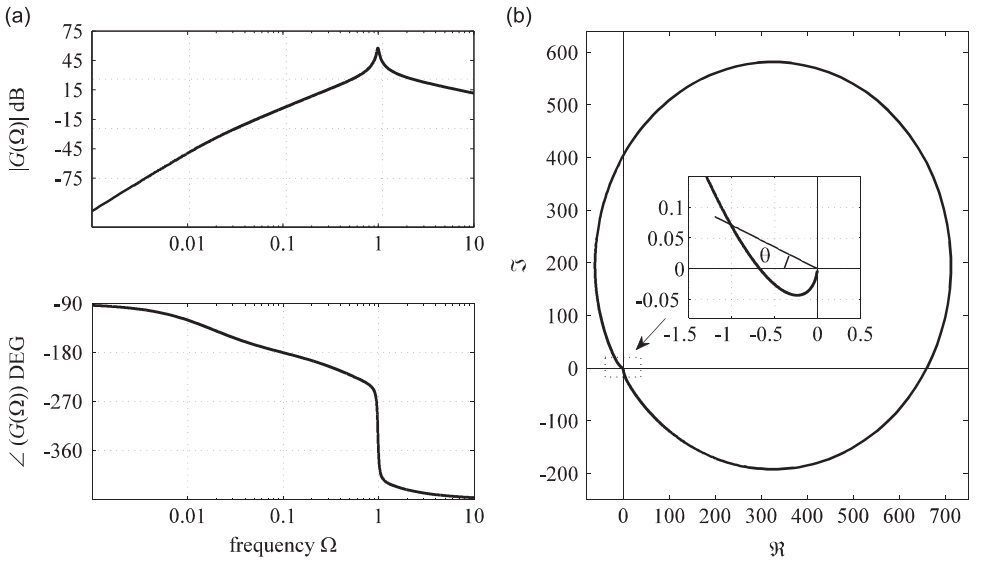

Fig. 6. (a) Magnitude and phase plots and (b) Nyquist plot for the sensor–actuator open loop frequency response function under the optimal setting with $\mu = 0.1$ and $f = 0.1$.

$G(\mathrm{i}\Omega)$ can be calculated as follows:

$$G(\mathrm{i}\Omega) = Y_{1,1}(\mathrm{i}\Omega) - Y_{1,2}(\mathrm{i}\Omega), \tag{25}$$

where $Y_{1,1}(\mathrm{i}\Omega)$ is the dimensionless driving point mobility of the primary structure, and $Y_{1,2}(\mathrm{i}\Omega)$ is the dimensionless transfer mobility between the force acting on the reaction mass and the primary structure velocity.

Expressions for $Y_{1,1}(\mathrm{i}\Omega)$and $Y_{1,2}(\mathrm{i}\Omega)$ in the case of the open loop ($g=0$) are as follows:

$$Y_{1,1}(\mathrm{i}\Omega) = \frac{(\Omega^2 - f^2 - 2\mathrm{i}\Omega\eta f)\Omega}{2\eta f(1+\mu)\Omega^3 - 2\eta f\Omega + \mathrm{i}(\Omega^4 - (1+(1+\mu)f^2)\Omega^2 + f^2)}, \tag{26}$$

$$Y_{1,2}(\mathrm{i}\Omega) = \frac{(-f - 2\mathrm{i}\Omega\eta)\Omega f}{2\eta f(1+\mu)\Omega^3 - 2\eta f\Omega + \mathrm{i}(\Omega^4 - (1+(1+\mu)f^2)\Omega^2 + f^2)}. \tag{27}$$

The dimensionless frequency response function of the feedback controller is given by

$$H(\mathrm{i}\Omega) = 2\mu f\eta\xi. \tag{28}$$

The open loop frequency response, $G(\mathrm{i}\Omega)H(\mathrm{i}\Omega)$, can thus be expressed as

$$G(i\Omega)H(\mathrm{i}\Omega) = \frac{2\mu f\xi\eta\Omega^3}{2\eta f(1+\mu)\Omega^3 - 2\eta f\Omega + \mathrm{i}(\Omega^4 - (1+(1+\mu)f^2)\Omega^2 + f^2)}. \tag{29}$$

The magnitude, phase and Nyquist plots of the open loop frequency response, $G(\mathrm{i}\Omega)H(\mathrm{i}\Omega)$, are shown in Fig. 6, where η and ξ are set to their optimal values given in Eqs. (14) and (15), respectively, with $\mu = 0.1$ and $f = 0.1$. The phase margin is marked as the angle θ in Fig. 6(b).

By substituting Eq. (29) into Eq. (23) the phase margin can be calculated as

$$\mathrm{PM} = \pi + \angle\left\{\frac{2\mu f\xi\eta\Omega_{\mathrm{gc}}^3}{2\eta f(1+\mu)\Omega_{\mathrm{gc}}^3 - 2\eta f\Omega_{\mathrm{gc}} + \mathrm{i}(\Omega_{\mathrm{gc}}^4 - (1+(1+\mu)f^2)\Omega_{\mathrm{gc}}^2 + f^2)}\right\}. \tag{30}$$

If η and ξ are set to their optimal values, the phase margin can be calculated only in terms of the non-dimensional gain crossover frequency, the mass ratio and the frequency ratio:

$$\mathrm{PM} = \pi + \angle\left\{\frac{2\sqrt{3}\Omega_{\mathrm{gc}}^3}{9f^2(\sqrt{3}}/3(-1+(\mu+1)\Omega_{\mathrm{gc}}^2)\Omega_{\mathrm{gc}} + \mathrm{i}(\Omega_{\mathrm{gc}}^4 - (1+(\mu+1)f^2)\Omega_{\mathrm{gc}}^2 + f^2))\right\}. \tag{31}$$

The frequencies Ω_{gc} that satisfy Eq. (24) can be calculated as the roots of the following polynomial:

$$\begin{aligned} &9f^4(3\Omega^8 + ((-6-6\mu)f^2 - 5 + 2\mu + \mu^2)\Omega^6 \\ &+ (3(1+\mu)^2f^4 + (6\mu+12)f^2 - 2\mu + 1)\Omega^4 \\ &+ (1 + (-6-6\mu)f^4 - 6f^2)\Omega^2 + 3f^4) - 4\Omega^6 = 0. \end{aligned} \tag{32}$$

Since the polynomial in Eq. (32) is bi-quartic, it is not practical to calculate explicit expressions for the roots. However, if the frequency ratio is significantly smaller than one, the left-hand side of Eq. (32) can be expanded into Taylor series with respect to the frequency ratio f around zero which yields

$$3\Omega^6+\left(\mu^2+2\mu-5-\frac{4}{9f^4}\right)\Omega^4+(1-2\mu)\Omega^2+1=0. \tag{33}$$

The Taylor expansion is applied to the smaller positive real root to obtain

$$\Omega_{\mathrm{gc},1}=\frac{\sqrt{6}}{2}f+O(f^3). \tag{34}$$

The open loop frequency response, $G(\mathrm{i}\Omega)H(\mathrm{i}\Omega)$, at the gain crossover frequency $\Omega_{\mathrm{gc},1}$ can be then expressed as

$$G(\mathrm{i}\Omega_{\mathrm{gc},1})H(\mathrm{i}\Omega_{\mathrm{gc},1})=-1-f^2-\frac{3\mu f^2}{2}+\frac{\sqrt{2}f}{2}\mathrm{i}+O(f^3). \tag{35}$$

The absolute value of the phase margin is then calculated using Eq. (23) and neglecting the higher-order terms:

$$|\mathrm{PM}|\approx\frac{\sqrt{2}f}{2} \tag{36}$$

which is valid if the frequency ratio f is significantly smaller than one. The relative error introduced by the approximation is less than 3 percent up to the mass ratio and the frequency ratios of 20 percent.

In conclusion, in order to get a larger phase margin, the frequency ratio f should be increased. However, as can be seen in Fig. 2, the optimal performance index $I^{\mathrm{IA}}_{k,\mathrm{opt}}$ in Eq. (13) increases with an increase in the frequency ratio f degrading the control performance. Therefore, there is a trade-off in choosing a suitable frequency ratio f. For better control performance it should be decreased, whereas for better robustness in terms of the phase margin it should be increased.

In the next section the control performance achieved using optimally tuned inertial actuators is compared to that achieved using optimally tuned mass dampers, according to Warburton [24]. The frequency ratio in the case of the control using IAs depends on the design of the actuator, but it is assumed that it can be set to a value significantly below unity. Since the frequency ratio is a compromise between the relative stability requirements and the control performance, the TMD/IA comparison results are expressed as a function of the frequency ratio.

5. Comparison of the passive control effect using TMDs and active control effects using IAs

Next, the vibration control effects obtained with IAs are compared to those obtained with TMDs. In order to do this, the Control Performance Ratio (CPR) is defined as

$$\mathrm{CPR}=\frac{I^{\mathrm{IA}}_{k,\mathrm{opt}}}{I^{\mathrm{TMD}}_{k,\mathrm{opt}}}, \tag{37}$$

where $I^{\mathrm{TMD}}_{k,\mathrm{opt}}$ is the performance index corresponding to an optimally configured passive TMD, such that the stiffness and the damping coefficient of the TMD are set to minimise the kinetic energy of the primary structure per white noise excitation [24]. The optimal parameters for the TMD and $I^{\mathrm{TMD}}_{k,\mathrm{opt}}$ are listed in Table 1.

After substituting from Eq. (13) and Table 1, the CPR is developed into Taylor series around $f=0$:

$$\mathrm{CPR}=(3\sqrt{3})/2f^2\sqrt{(\mu(\mu+1))}+O(f^4). \tag{38}$$

Table 1
Summary of the optimal parameters derived under $\mathcal{H}_2$ optimisation criterion for TMDs and IAs.

Optimal parameters	TMD[a]	IA[b] ($\mu\ll1, f\ll1$)
Passive damping ratio	$\frac{\sqrt{\mu}}{2}$	$\frac{\sqrt{3}}{6f}$
Frequency ratio	$\frac{1}{\sqrt{\mu+1}}$	$\ll1$
Active to passive damping ratio	–	$\frac{2}{3\mu f^2}$
Performance index	$\frac{2\pi}{\sqrt{\mu(\mu+1)}}$	$3\pi\sqrt{3}f^2$
Gain margin (dB)	–	3.5
Phase margin (radians)	–	$\frac{\sqrt{2}}{2}f$

[a] Warburton [24].
[b] This study.

Thus, the Control Performance Ratio for low frequency, lightweight IAs expressed in dBs is

$$\mathrm{CPR} \approx 4,15 + 5\log_{10}[\mu(\mu+1)] + 20\log_{10} f. \tag{39}$$

It is possible to see from Eq. (39) that halving the frequency ratio of an IA gives an extra 6 dB vibration reduction over the optimally tuned passive absorber having the same mass, and decimating it gives an extra 20 dB reduction. This is illustrated in Fig. 7, where the Control Performance Ratio is plotted against the frequency ratio for various mass ratios.

It can be noted in Fig. 7 that the improvement achieved using the active control over the passive control approach is more evident for a smaller added mass of the device.

Finally, the two control methods are compared on an example system, and the effects of adding either an optimally tuned TMD or an optimally tuned IA onto an undamped primary structure are illustrated. The mass ratio μ is assumed to be 0.1 for both cases, and the frequency ratio f for the passive TMD is calculated according to [24] (Table 1), while for the active IA the frequency ratio f is set to 0.1. Fig. 8(a) shows the amplitude of the primary structure driving point mobility plotted against the dimensionless frequency for the two cases.

It can be seen that the amplitude of the driving point mobility in the case of the passive control is higher than the amplitude of the driving point mobility in the case of the active control at all frequencies except around the resonance frequency of the IA. This is due to the fact that the active control generates control spillover at frequencies around the inertial actuator resonance. Thus the optimal active control is a trade-off between the vibration reduction at around the resonance frequency of the actuator and that around the resonance frequency of the primary structure. This compromise, however, can be achieved with significant improvement in vibration reduction over the passive control approach.

In Fig. 8(b) a case is considered where the resonance frequency of the IA is increased to be the same as the optimal resonance frequency of the TMD. The optimal passive and active damping ratios are set according to Eqs. (11) and (12). This situation is relevant if the vibration reduction performance of the active system is to be preserved in case of power supply disruption. It can be seen that with increased resonance frequency the benefits of using the active control are lost and the two dashed lines in plots (a) and (b) are nearly the same.

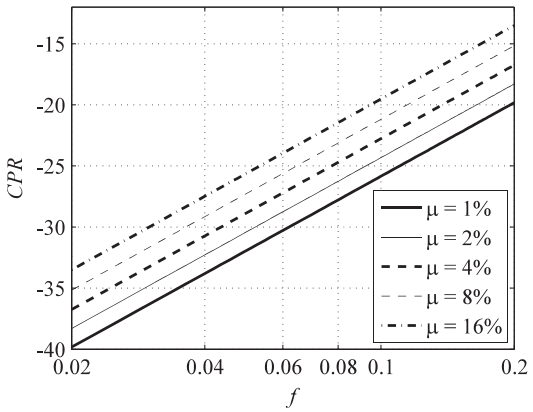

Fig. 7. The ratio of the control performance (CPR) between $\mathcal{H}_2$ optimally tuned IAs and TMDs for different mass ratios, as a function of the frequency ratio.

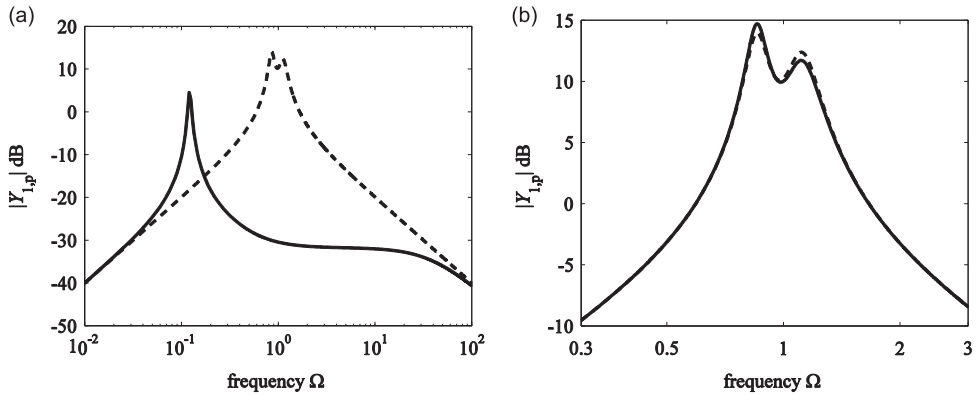

Fig. 8. The amplitude of the primary structure driving point mobility plotted against the dimensionless frequency. Plot (a) dashed line is for an optimally tuned mass damper and the solid line is for an optimally tuned IA having a resonance frequency 1/10th the resonance frequency of the primary structure. Plot (b) the solid line is for an optimally tuned IA having an increased resonance frequency such that it is the same as the optimal resonance frequency of the TMD and the dashed line is the same IA when the active control ratio is zero due to a possible power supply disruption.

6. Conclusions

The optimal tuning parameters for the active control using IAs are derived and summarised in Table 1. These are the passive damping of the actuator dashpot and the active damping determined through the velocity feedback gain. There is no optimal resonance frequency for the active control using IAs; instead it should be as far below the resonance frequency of the primary structure as practically possible. Depending on how low the frequency ratio can be, the active control can outperform the passive control for the same added mass. Halving the frequency ratio gives an extra 6 dB vibration reduction; decimating it gives an extra 20 dB reduction. The improvement in the vibration reduction using the active control over the passive control is more evident for a smaller proof mass. In the case of the active control the gain margin is constant and equals 3.5 dB. The phase margin decreases linearly with a decrease in the frequency ratio. It is noted that the optimal active control is a trade-off between the vibration reduction at around the resonance frequency of the actuator and that around the resonance frequency of the primary structure. Also the frequency ratio is a trade-off between the control performance and the relative stability in terms of the phase margin.

Acknowledgements

The research performed by Neven Alujević was financially supported through an EU FP7 Marie Curie Industry-Academia Partnerships and Pathways (IAPP) Grant Agreement 251211. The research performed by Guoying Zhao was financed by the China Scholarship Council (Grant No: 2010611008). Also the Agentschap voor Innovatie door Wetenschap en Technologie (IWT) Flanders (Grant No: IWT/120029) within the OptiWind project is gratefully acknowledged for support to Guoying Zhao.

Appendix A

In this appendix to the paper it is shown that the difference between the right-hand sides of inequalities (19) and (18) is positive, or, in other words, the stability criterion given in Eq. (19) is the stricter one. The difference E is given by

$$E=\frac{-\mu f^2-f^2+1-\sqrt{(-\mu f^2-f^2+1)^2+4\mu f^2}}{2\mu f^2}+1+\frac{1}{\mu}-\frac{1}{\mu(\mu f^2+f^2+1)}. \tag{A1}$$

By grouping together the first three terms of the right-hand side of Eq. (A1), the difference E takes the form

$$E=\frac{\mu f^2+f^2+1-\sqrt{(-\mu f^2-f^2+1)^2+4\mu f^2}}{2\mu f^2}-\frac{1}{\mu(\mu f^2+f^2+1)}. \tag{A2}$$

The expression inside the square root in Eq. (A2) can be reassembled as

$$\sqrt{(-\mu f^2-f^2+1)^2+4\mu f^2}=\sqrt{(\mu f^2+f^2+1)^2-4f^2}. \tag{A3}$$

E is then rewritten as

$$E=\frac{\mu f^2+f^2+1-\sqrt{(\mu f^2+f^2+1)^2-4f^2}}{2\mu f^2}-\frac{1}{\mu(\mu f^2+f^2+1)}. \tag{A4}$$

By grouping the right-hand side of Eq. (A4) one can obtain

$$E=\frac{\mu f^2+f^2+1-\sqrt{(\mu f^2+f^2+1)^2-4f^2}}{\mu(\mu f^2+f^2+1)(\mu f^2+f^2+1+\sqrt{(\mu f^2+f^2+1)^2-4f^2})}, \tag{A5}$$

where both the numerator and the denominator can be multiplied by $\mu f^2+f^2+1+\sqrt{(\mu f^2+f^2+1)^2-4f^2}$ such that the difference E takes the following form:

$$E=\frac{4f^2}{\mu(\mu f^2+f^2+1)(\mu f^2+f^2+1+\sqrt{(\mu f^2+f^2+1)^2-4f^2})^2}. \tag{A6}$$

Since μ and f are both positive, it can be seen from Eq. (A6) that the difference E between the right-hand sides of inequalities (19) and (18) is always positive.

References

[1] J. Ormondroyd, J.P. den Hartog, The theory of the vibration absorber, *Transactions of the American Society of Mechanical Engineers* 49 (1928) A9–A22.
[2] J.B. Hunt, *Dynamic Vibration Absorbers*, Mechanical Engineering Publications Ltd., London, 1979.
[3] D.J. Mead, *Passive Vibration Control*, Wiley, New York, 1999.

[4] J.P. Den Hartog, *Mechanical Vibrations*, McGraw-Hill Book Co., New York, 1934.
[5] H. Frahm, Devices for damping vibrations of bodies, U.S. Patent No. 989,958, 1911.
[6] J. van Dyke, J. Schendel, C. Gunderson, M. Ballard, Cabin Noise Reduction in the DC-9, AIAA Paper 67-401, 1967.
[7] J.Q. Sun, M.R. Jolly, M.A. Norris, Passive, adaptive and active tuned vibration absorbers – a survey, *Transactions of American Society of Mechanical Engineers Journal of Mechanical Design* 117 (1995) 234–242.
[8] A.H. von Flotow, A. Beard, D. Bailey, Adaptive tuned vibration absorbers: tuning laws, tracking agility, sizing and physical implementations, *Proceedings of Noise – Conference* 94 (1994) 437–454.
[9] M.J. Brennan, Vibration control using a tunable vibration neutralizer, *Proceedings of the Institution of Mechanical Engineers, Journal of Mechanical Engineering Science* 211 (1997) 91–108.
[10] P.L. Walsh, J.S. Lamancusa, A variable stiffness vibration absorber for the minimisation of transient vibrations, *Journal of Sound and Vibration* 158 (1992) 195–211.
[11] M.J. Brennan, Actuators for active vibration control – tunable resonant devices, *Proceedings of the Fourth European Conference on Smart Materials and Structures*, Harrogate, UK, 6–8 July 1998, pp. 41–48.
[12] C.Q. Howard, Review of adaptive tuned vibration neutralisers, *Proceedings of Acoustics 2009: Research to Consulting, the Annual Conference of the Australian Acoustical Society*, University of Adelaide, 23–23 November 2009, pp. 1–6.
[13] M.W. Ryan, M.A. Franchek, R. Bernhard, Adaptive-passive vibration control of single frequency excitations applied to noise control, *1994 Noise-Con Proceedings*, Ft. Lauderdale, Florida, May 1994, pp. 461–466.
[14] M.A. Franchek, M.W. Ryan, R.J. Bernhard, Adaptive passive vibration control, *Journal of Sound and Vibration* 189 (1995) 565–585.
[15] E. Rustighi, M.J. Brennan, B.R. Mace, A shape memory alloy adaptive tuned vibration absorber: design and implementation, *Smart Materials and Structures* 14 (2005) 19–28.
[16] K. Williams, G. Chiu, R. Bernhard, Adaptive-passive absorbers using shape-memory alloys, *Journal of Sound and Vibration* 249 (5) (2002) 835–848.
[17] C.L. Davis, G.A. Lesieutre, An actively tuned solid-state vibration absorber using capacitive shunting of piezoelectric stiffness, *Journal of Sound and Vibration* 232 (3) (2000) 601–617.
[18] R.A. Morgan, K.W. Wang, An active–passive piezoelectric absorber for structural vibration control under harmonic excitations with time-varying frequency, part 1: algorithm development and analysis, *Journal of Vibration and Acoustics – Transactions of the ASME* 124 (1) (2002) 77–83.
[19] R.A. Morgan, K.W. Wang, An active–passive piezoelectric absorber for structural vibration control under harmonic excitations with time-varying frequency, part 2: experimental validation and parametric study, *Journal of Vibration and Acoustics – Transactions of the ASME* 124 (1) (2002) 84–89.
[20] N. Alujević, I. Tomac, P. Gardonio, Tuneable vibration absorber using acceleration and displacement feedback, *Journal of Sound and Vibration* 331 (12) (2012) 2713–2728.
[21] J. Tang, K.W. Wang, Active–passive hybrid piezoelectric networks for vibration control: comparisons and improvement, *Smart Materials and Structures* 10 (4) (2001) 794–806.
[22] F. Weber, M. Maslanka, Frequency and damping adaptation of a TMD with controlled MR damper, *Smart Materials and Structures* 21 (2012) 055011.
[23] O. Nishihara, T. Asami, Closed-form solutions to the exact optimizations of dynamic vibration absorbers (minimizations of the maximum amplitude magnification factors), *Journal of Vibration and Acoustics* 124 (2002) 576–582.
[24] G.B. Warburton, Optimum absorber parameters for various combinations of response and excitation parameters, *Earthquake Engineering and Structural Dynamics* 10 (1982) 381–401.
[25] Y. Iwata, On the construction of the dynamic vibration absorber, *Japanese Society of Mechanical Engineering* 820 (1982) 150–152.
[26] H. Yamaguchi, Damping of transient vibration by a dynamic absorber, *Transactions of the Japan Society of Mechanical Engineers, Series C* 54 (1988) 561–568.
[27] D.W. Miller, E.F. Crawley, B.A. Wards, Inertial actuator design for maximum passive and active energy dissipation in flexible space structures, *Proceedings of Structures, Structural Dynamics, and Materials Conference American Institute of Aeronautics and Astronautics*, Orlando, FL, April 1985, pp. 536–544.
[28] S. Krenk, Frequency analysis of the tuned mass damper, *Journal of Applied Mechanics* 72 (2005) 936–942.
[29] M. Zilletti, S.J. Elliott, E. Rustighi, Optimisation of dynamic vibration absorbers to minimise kinetic energy and maximise internal power dissipation, *Journal of Sound and Vibration* 331 (2012) 4093–4100.
[30] C. Paulitsch, P. Gardonio, S.J. Elliott, P. Sas, R. Boonen, Design of a lightweight, electrodynamic, inertial actuator with integrated velocity sensor for active vibration control of a thin lightly-damped panel, *Proceedings of the International Conference on Noise and Vibration Engineering (ISMA)*, Katholieke Universiteit Leuven, Belgium, 20–23 September 2004.
[31] C. Paulitsch, P. Gardonio, S.J. Elliott, Active vibration control using an inertial actuator with internal damping, *Journal of the Acoustical Society of America* 119 (2006) 2131–2140.
[32] S.J. Elliott, M. Serrand, P. Gardonio, Feedback stability limits for active isolation systems with reactive and inertial actuators, *Journal of Vibration and Acoustics* 123 (2001) 250–261.
[33] N. Alujević, H. Wolf, P. Gardonio, I. Tomac, Stability and performance limits for active vibration isolation using blended velocity feedback, *Journal of Sound and Vibration* 330 (21) (2011) 4981–4997.
[34] D.E. Newland, *An Introduction to Random Vibrations, Spectral and Wavelet Analysis*, 3rd ed. Dover Publications, Inc., Mineola, New York, 2012.
[35] L. Meirovitch, *Dynamics and Control of Structures*, Wiley Interscience, New York, 1990 (425 pp).